Scaling Efficient Masked Autoencoder Learning on Large Remote Sensing Dataset

Fengxiang Wang[1], Hongzhen Wang[2]*, Di Wang[3], Zonghao Guo[4], Zhenyu Zhong[5],
Long Lan[1]*, Jing Zhang[6], Zhiyuan Liu[2], Maosong Sun[2]

[1] National University of Defense Technology, China [2] Tsinghua University, China
[3] Wuhan University, China [4] University of Chinese Academic of Sciences, China
[5] Nankai University, China [6] The University of Sydney, Australia

Abstract

Masked Image Modeling (MIM) has emerged as a pivotal approach for developing foundational visual models in the field of remote sensing (RS). However, current RS datasets are limited in volume and diversity, which significantly constrains the capacity of MIM methods to learn generalizable representations. In this study, we introduce **RS-4M**, a large-scale dataset designed to enable highly efficient MIM training on RS images. RS-4M comprises 4 million optical images encompassing abundant and fine-grained RS visual tasks, including object-level detection and pixel-level segmentation. Compared to natural images, RS images often contain massive redundant background pixels, which limits the training efficiency of the conventional MIM models. To address this, we propose an efficient MIM method, termed **SelectiveMAE**, which dynamically encodes and reconstructs a subset of patch tokens selected based on their semantic richness. SelectiveMAE roots in a progressive semantic token selection module, which evolves from reconstructing semantically analogical tokens to encoding complementary semantic dependencies. This approach transforms conventional MIM training into a progressive feature learning process, enabling SelectiveMAE to efficiently learn robust representations of RS images. Extensive experiments show that SelectiveMAE significantly boosts training efficiency by 2.2-2.7 times and enhances the classification, detection, and segmentation performance of the baseline MIM model. The dataset, source code, and trained models will be released at RS-4M.

1 Introduction

Over the past decade, advancements in remote sensing (RS) technology and data acquisition have significantly improved applications in ecosystem monitoring [1], natural disaster management [2], among others [3, 4]. These applications rely on essential capabilities such as scene classification [5, 6], object detection [7], change detection [8], and semantic segmentation [9]. However, each of these downstream tasks often requires substantial computational resources to learn task-specific feature representations and develop specialized models.

Thanks to significant advances in self-supervised learning methods, such as Masked Image Modeling (MIM) techniques [10, 11], the pre-training of visual foundation models has seen remarkable improvements [12–17]. Consequently, remote sensing foundation models (RSFMs) have recently emerged, offering general feature representations and achieving outstanding performance across various remote sensing downstream tasks [18]. However, two challenges persist in the development of RSFMs. (i) Compared to the ImageNet-21k [19] dataset, previous RS datasets [20–23] contain significantly fewer

---

*Corresponding Authors

Preprint.

samples (approximately 1 million vs. 14 million), which impedes the sufficient MIM training of large backbones. (ii) These datasets, which primarily focus on global scene semantics [20–22], lack the diversity and fine-grained information of RS scenarios encountered in downstream tasks. This limitation restricts the generalization of the learned representations.

To address these challenges, we introduce a large-scale RS dataset called **RS-4M**. This dataset, comprising 4 million optical images, is designed to fully leverage the representation learning capabilities of MIM methods in RS applications. RS-4M significantly exceeds previous RS datasets [24, 21, 25–36, 18, 37, 38], being at least four times larger. Moreover, RS-4M encompasses a wide range of diverse RS scenarios encountered in downstream tasks such as object-level detection and pixel-level segmentation (Fig. 1 left).

Despite substantial efforts in training RSFM using MIM methods, such as leveraging general image knowledge [25, 26, 28], expanding parameter scales [29], integrating spatio-temporal information [30–32], and learning multi-scale features [33, 35, 36], the significant computational burden and slow convergence when employing MIM training on large-scale RS datasets cannot be ignored. Specifically, pre-training on 1 million RS samples requires 107 hours for the ViT-B [39] backbone on 8 Nvidia A100 GPUs [18]. In natural scene analysis, this issue has led to numerous studies [40–45] aimed at improving MIM training efficiency. One approach is to accelerate the token reconstruction process by using decoders with fewer parameters [40, 41]. Another approach is to reduce the number of visible patch tokens input into the vision encoder [42–44], significantly speeding up feature extraction.

However, conventional MIM approaches, such as the encoding-then-decoding procedure, overlook the unique characteristics of RS images, which typically feature sparse foreground pixels and dense backgrounds [18, 28]. This raises two key questions about how to efficiently conduct MIM training in the RS field: **(i) Is it necessary to reconstruct all the redundant background patches during the MIM decoding process? (ii) Is there a feasible way to encode fewer image patches ($e.g.$, $\leq 25\%$) to accelerate the convergence of MIM training?** To address the first question, a measure-based selection process is needed to identify the appropriate patches for reconstruction. For the second question, the intuition is that the patch tokens used in the encoding-then-decoding procedure should effectively capture feature dependencies in RS images.

We propose an efficient MIM method called SelectiveMAE, which dynamically encodes and reconstructs patch tokens based on their semantic richness. Specifically, SelectiveMAE utilizes the Histogram of Oriented Gradients (HOG) algorithm to quantify the semantic richness of patches. Then, it selects a subset of patch tokens ($e.g.$, $\leq 50\%$) with higher HOG values for feature encoding ($e.g.$, $\leq 15\%$) and pixel reconstruction ($e.g.$, $\leq 35\%$). However, using an extremely low ratio of visible patches during MIM training can lead to gradient explosion or vanishing (Fig. 3). To mitigate this, we designed a Progressive Semantic Token Selection (PSTS) module, which dynamically leverages semantically relevant patch tokens throughout the entire MIM training phase. At the beginning, SelectiveMAE encodes semantically rich tokens and reconstructs semantically similar ones to warm up the training process. As training advances, SelectiveMAE shifts to reconstructing high-semantic tokens from encoded lower-semantic ones to capture complementary semantic dependencies. This analogical-to-complementary approach allows SelectiveMAE to efficiently and progressively learn robust representations of RS images, thereby accelerating MIM convergence. Our experiments reveal that only 40% of RS image patches are sufficient to train a comparable MIM model, offering new insights into conducting MIM training on RS images.

The contributions of this paper are summarized as follows. **(1)** We introduce the RS-4M dataset, a large-scale optical remote sensing dataset for unsupervised learning methods to date, distinguished by its diverse scene details. **(2)** We propose SelectiveMAE, a novel and efficient MIM method tailored for remote sensing images. This method incorporates a new PSTS module, which significantly accelerates convergence and enhances representation learning compared to the original MIM approach.

Experiment results suggest that compared to the baseline method, SelectiveMAE not only achieves $2.2 - 2.7\times$ speedup in pre-training but also provides performance improvement of 5.6% mAP and 1.4% mF1 when applied to downstream object detection and segmentation tasks, respectively.

2 Related Work

Remote Sensing Datasets. In recent years, many RS datasets have been created for tasks such as scene classification [23, 46], object detection [47–49], and segmentation [50–52]. The availability of free, unlabeled satellite images has led to the development of large-scale RS datasets. Some works, like SEN12MS [53] with 180,662 triplets of dual-pol synthetic aperture radar (SAR) and multi-spectral Sentinel-2 image patches, combine various sensor data to create extensive datasets, while many other datasets focus solely on optical RS images. MillionAID [20] offers a million-scale dataset for RS optical image classification, while SeCo [22] and CACo [21] provide nearly a million images of the same location over different times. These datasets primarily target scene classification and often overlook fine-grained target information, limiting their utility for various downstream tasks. To address this gap, we introduce the RS-4M dataset, which is larger and more diverse, enhancing performance across multiple downstream tasks.

Remote Sensing Foundation Models. remains unlabeled and thus inaccessible for supervised learning [54]. Self-supervised learning methods have recently been employed to extract representations from unlabeled RS data. Although there are some contrastive self-supervised methods [24, 21, 22, 55], recent advancements have primarily centered around generative self-supervised methods. For example, RVSA [18] leverages the vision transformer backbone pre-trained by the vanilla MAE [10] method and introduces computationally efficient rotated varied-size window attention to replace the original attention during fine-tuning. In addition, many studies are focusing on improving generative self-supervised algorithms by leveraging general image knowledge [25, 26, 28], scaling up parameter sizes [29], integrating spatio-temporal data [30–32], handling multi-sensor data [56–60], and employing multi-scale concepts [33, 35, 36]. However, these methods have not effectively addressed the substantial computational burden associated with self-supervised pre-training in RS. In this paper, we propose a novel acceleration method that significantly speeds up training, enhancing practicality in the RS domain.

Masked Image Modeling. Inspired by the success of Masked Language Modeling (MLM) in NLP [61], MIM has been developed for visual pre-training [62, 11, 10, 63, 64]. MIM learns image representations by reconstructing masked tokens, focusing on various regression targets [65–69], masking strategies [70, 71], and reconstruction methods [72–75]. For instance, MAE [10] demonstrates that predicting pixel values can be as effective as using complex targets. A major challenge for MIM is its high computational demand and lengthy pre-training times. To mitigate this, some studies use asymmetric encoder-decoder strategies [40, 41], reduce input patches [42, 44] or ues a novel Difficulty-Flatten Loss [43]. Additionally, CrossMAE [45] employs cross-attention between masked and visible tokens to enhance efficiency without sacrificing performance. However, these methods do not account for the unique characteristics of RS images, such as sparse foreground information and complex backgrounds. In this paper, we introduce a novel PSTS module to address this issue and accelerate the training process.

3 Dataset

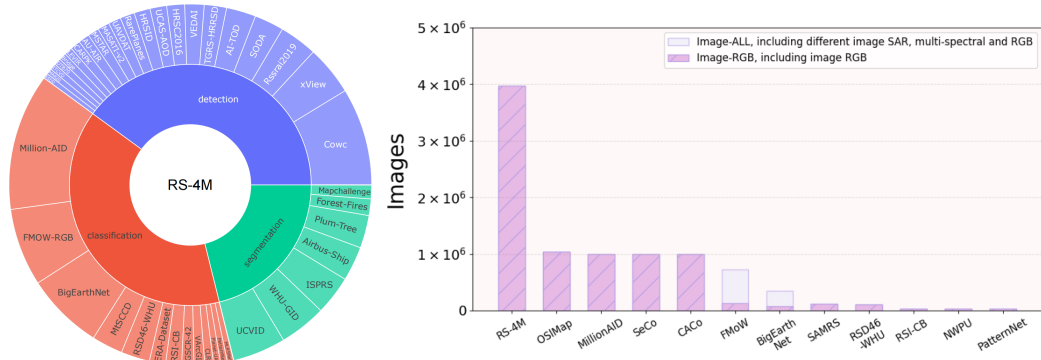### 3.1 Data collection and organization

Figure 1: **Left**: The organization of data sources in RS-4M. **Right**: The comparison between RS-4M and other datasets.

Recent advancements in self-supervised pre-training RSFMs are hindered by the smaller scale and diversity of existing RS datasets compared to natural scene datasets. To address this issue, we propose the RS-4M dataset, a continuously updated large-scale RS dataset following the principles of Diversity, Richness, and Scalability (DiRS) [20]. (1) We collected and organized datasets from the past decade, focusing on mainstream RS image interpretation tasks, including scene classification, object detection, semantic segmentation, and change detection. These datasets, detailed in Fig. 1, encompass around 100 sub-datasets with a total of 13.5 million images. (2) We excluded multispectral and SAR data, keeping only optical images in this study. Future updates will incorporate multispectral and SAR data to support multi-modal self-supervised pre-training. (3) Unlike datasets like MillionAID [20] designed for scene classification, our RS dataset is designed to facilitate downstream detection and segmentation tasks. To address large-scale image in segmentation datasets, we randomly cropped high-resolution images into smaller slices. (4) Images with pixels below 64 or above 1024 were removed to facilitate self-supervised pre-training. (5) We combined the remaining images and eliminated duplicates using a two-phase process: a coarse phase with perceptual hashing[76] and a refined phase with manual review. With the Hash value to select and the checking of manual review, only highly similar images are excluded. This resulted in the RS-4M dataset containing about 4 million high-quality RS optical images, which is four times larger than previous representative RS datasets, as shown in Fig. 1 right.

Table 1: Comparison between RS-4M and MillionAID: ViT Base models [39] are pre-trained on these datasets using MAE [10] and fine-tuned on the RESISC-45 dataset [77].

Dataset	Images Number	Epoch	Top-1 Accuracy
MillionAID [20]	1 Million	800	89.20
RS-4M	2 Million	400	91.80
RS-4M	3 Million	267	92.24
RS-4M	**4 Million**	**200**	**92.38**

3.2 Preliminary Evaluation of RS-4M Dataset

RS-4M offers a significantly larger and more diverse image set compared to previous datasets. To evaluate its effectiveness, we pre-train a ViT base model [39] using the vanilla MAE method [10]. For comparison, we use the MillionAID dataset, maintaining an equal number of data points during training: 800 epochs for MillionAID's 1 million images and 200 epochs for our RS-4M dataset. In addition, we create new datasets by sampling different numbers of images from RS-4M for further comparison. After pre-training, we fine-tune the models on the downstream RESISC-45 dataset [77] and assess the Top-1 classification accuracy. The results in Table 1 demonstrate that the RS-4M dataset outperforms MillionAID across various sample sizes, with the highest accuracy of 92.38% achieved using the entire dataset. Even with fewer images, RS-4M consistently delivers superior performance, highlighting its greater diversity and effectiveness. These findings underscore the advantage of using larger and more varied datasets for unsupervised pre-training.

4 Method

4.1 Masked Autoencoders Preliminaries

1) Masking. Similar to supervised training of a standard ViT, MAE divides the image into regular, non-overlapping patches. It then samples a subset of these patches and masks the remaining ones. Typically, the masking ratio is 75%, meaning only 25% of the patches are input to the encoder. This random sampling follows a uniform distribution according to the masking ratio. **2) MAE Encoder.** The encoder is a standard ViT applied only to the visible, unmasked patches. It linearly projects the patches, adds positional embeddings, and processes them through a series of transformer blocks. By operating on a smaller subset of patches, the encoder enables training of large models with reduced computational and memory requirements. **3) MAE Decoder.** The encoded tokens and masked tokens are fed into the decoder, which comprises transformer blocks with self-attention layers. The masked tokens are shared, learnable tensors enhanced with positional embeddings. The decoder, utilized only during pre-training, generates the output predictions for those masked tokens. **4) Reconstruction Target.** MAE predicts the pixel values for each masked patch, with each element in the decoder output representing a patch's pixel value vector. The loss function computes the mean squared error (MSE) between the reconstructed targets and original patches.

RS optical images typically contain many redundant background pixels, which aligns well with MAE's masking strategy. In MAE, the encoder processes only 25% of the patches, significantly reducing computational load by avoiding processing the entire image. Building on MAE, we aim to leverage the redundancy in RS images to accelerate training. Specifically, we address two questions: *1) Is it necessary to reconstruct all the masked patches given the redundancy in RS images? 2) Can the visible patches input to the MAE encoder be further compressed to enhance acceleration?*
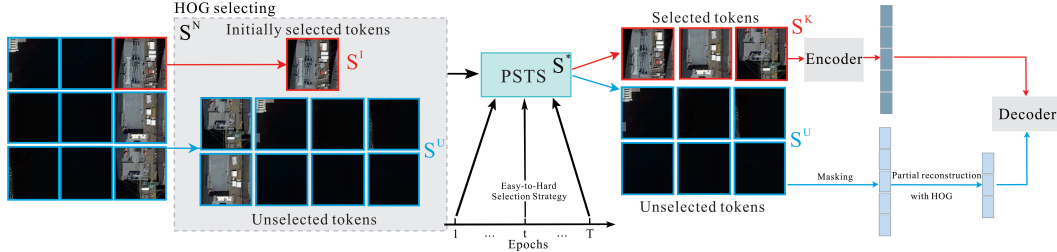

Figure 2: **Overview of SelectiveMAE.** The vanilla version of SelectiveMAE.

4.2 Partial Reconstruction

For question 1, previous research [45] has shown that for general images, when MAE reconstructs 75% of the patches to calculate the loss, a specially designed decoder doesn't need to fully reconstruct all remaining patches. In fact, reconstructing just 50% or even 25% of the patches can achieve similar performance and speed up training. However, for RS images, if we randomly sample patches and remove most for reconstruction, the reconstructed patches might not be semantically rich ones. As shown in Table 2, using only a random subset for reconstruction degrades performance.

Table 2: Results of different partial reconstruction strategies. Reconstruction Ratio=25%. Top-1 classification accuracy on RESISC-45 [77] is reported.

Method	Selection	Data Throu. /Min.	Acc.
Partial Reco.	False	17k	89.2
Partial Reco.	Random	25k	88.8
Partial Reco.	ATS [78]	20k	85.7
Partial Reco.	**HOG**	**25k**	**89.2**

To address this issue, we propose selecting semantically rich patches for reconstruction instead of random selection. Specifically, given an input image $x \in \mathbb{R}^{H \times W \times C}$, it is reshaped into $N = (H \times W)/p^2$ non-overlapping patches $x^p \in \mathbb{R}^{N \times (p^2 C)}$, where p is the patch size, (H, W) is the size of the input image, and C is the number of channels. These patches $\{x_i^p\}_{i=1}^N$ are then linearly mapped to patch embeddings. To retain positional information, positional embeddings are added to the patches. We select a portion of the patches to input to the encoder based on the masking ratio $m \in [0, 1]$ ($m = 85\%$ by default), as detailed in Sec. 4.1. The remaining patches serve as reconstruction targets for the decoder. Unlike MAE's masking ratio, we introduce a new reconstruction ratio r, the proportion of pixels to be reconstructed, denoted as $r \in [0, m]$ ($r = 25\%$ by default). We compute the HOG features $HOG(\cdot)$ of the remaining patches and select those with the high HOG feature values according to the reconstruction ratio r, rather than using all patches. The process can be formulated as:

$$token_R = \{x_i^p | i \in top_{\lfloor r \times N \rfloor}(HOG(\{x_i^p\}_{i=1}^{m \times N}))\}, \tag{1}$$

where $token_R$ denotes the selected mask tokens for reconstruction and $top_n(\cdot)$ denotes the index set of the selected top n tokens. The decoder uses a lightweight design based on cross-attention following CrossMAE [45]. Experimental results in Table 2 show that this partial reconstruction strategy significantly increases the training throughput without affecting the learned representations.

4.3 Progressive Semantic Token Selection

For the second question, we initially tried a naive approach by increasing the masking ratio to 85%, meaning only 15% of the patches in each RS image were input to the encoder while keeping a 25% reconstruction ratio as proposed in Sec. 4.2. However, during training, this setup often led to issues like gradient explosions or loss divergence, as shown in Fig. 3. To illustrate, we continued MAE's training despite these gradient explosions. The figure shows that using only 40% (=15%+25%) of the patches for encoding and reconstruction frequently caused unstable training due to gradient

5

explosions. We speculate that, although RS images have background redundancy, using such a small portion of patches significantly challenges MAE training.

How can we achieve acceleration at a high masking ratio (e.g., 85%) while ensuring MAE completes the pre-training task for RS images? Some studies suggest that machine learning algorithms often benefit from starting with simpler tasks and gradually increasing the difficulty, a strategy known as curriculum learning [79–81]. This approach involves progressively introducing more challenging examples during training. While curriculum learning typically focuses on whole image samples, self-supervised training, which masks large portions of image pixels, emphasizes patch-level selection. Therefore, in self-supervised training, it's essential to distinguish between "easy" and "hard" patches.

Figure 3: **Left**: Baseline training loss. Using only 40% of masked patches for reconstruction often leads to gradient explosions. **Right**: Training loss using PSTS.

To this end, we introduce the Progressive Semantic Token Selection (PSTS) module for patch selection. In this module, depicted in Fig. 2, we begin by selecting a limited number of patches and then select additional patches based on them in the training epoch, dynamically transitioning from easily learned, semantically similar patches to more challenging, complementary ones.

For initialization, we employ a HOG selection strategy to choose the initial patch set from $S^N = \{x_i^p\}_{i=1}^N$, with a proportion $s \in [0, (1-m)/2]$. We define the initial set of selected token as:

$$S^I = \{S^N(i) | i \in top_{\lfloor s \times N \rfloor}(HOG(S^N)\}. \tag{2}$$

We select $\lfloor s \times N \rfloor$ tokens with the maximum HOG feature values (*i.e.*, $top_{\lfloor s \times N \rfloor}$) from the original token set to form the initial token set. This simple yet effective strategy ensures that semantically rich tokens are selected.

Following token initialization, we aim to incrementally increase the number of tokens to facilitate a training progression from easy to difficult, while adhering to the final masking ratio for selected tokens. This process is outlined in Algorithm 1. Given the initial token sets' high HOG feature values, nearby tokens selected by PSTS also exhibit high HOG feature values. Recalling our partial reconstruction approach in Section 4.2, we filter the remaining unselected token set to include those with high HOG values as reconstruction targets. Consequently, when selecting nearby tokens, the tokens input for encoding and those chosen for reconstruction are closer, thereby simplifying the training process. Conversely, if a token's feature distribution significantly deviates from others in the set, indicating it is farther away, we consider such patches more challenging to learn.

Specifically, we select tokens from S^U based on S^I. First, we use $\mathbb{S}^\mathbb{I} \in \mathbb{R}^{|S^K| \times d}$ and $\mathbb{S}^\mathbb{U} \in \mathbb{R}^{|S^U| \times d}$ to denote the matrix representation of the initial token set S^I and the unselected token set S^U, where $|\cdot|$ represents the number of tokens and d the feature dimension after the embedding layer. We use Cosine Distance to measure the distance between the tokens in these two sets:

$$\mathcal{D}(S^U, S^I) = \mathbf{1} - cos\left\langle S^U, S^I \right\rangle = \mathbf{1} - \frac{\mathbb{S}^\mathbb{U}\mathbb{S}^{\mathbb{I}\mathrm{T}}}{\|\mathbb{S}^\mathbb{U}\| \cdot \|\mathbb{S}^\mathbb{I}\|}, \tag{3}$$

where $\mathbf{1}$ is an all-one matrix. $\mathcal{D}(S^U, S^I) \in \mathbb{R}^{|S^U| \times |S^I|}$ represents the pairwise distances between tokens in S^U and S^I. Next, we define the distance between the tokens in S^U to the initial token set S^K based on the selection criteria in each training stage as follows:

$$distance(S^U \to S^I)_i = \begin{cases} -\min_j(\mathcal{D}(S^U, S^I)_{i,j}), & \text{if } \zeta = 1, \\ \max_j(\mathcal{D}(S^U, S^I)_{i,j}), & \text{else if } \zeta = 2, \\ random_j(\mathcal{D}(S^U, S^I)_{i,j}), & \text{else}, \end{cases} \tag{4}$$

where $i \in \{1, \cdots, |S^U|\}$, $j \in \{1, \cdots, |S^I|\}$, and ζ represents the training stage depending on the number of epochs. Finally, we sample $\lfloor N \times (1-m-s) \rfloor$ tokens from S^U and add them with S^I to form S^K, which can be formulated as follows:

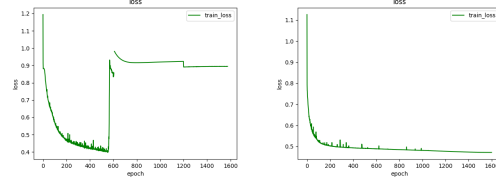$$S^* = \{S^U(i) | i \in top_{\lfloor N \times (1-m-s) \rfloor}(distance(S^U \to S^I)_i)\}, \tag{5}$$

6

Algorithm 1 Progressive Semantic Token Selection

Require: Number of training epochs T and total training stages N_g (*i.e.*, T/N_g epochs for each stage), masking rate m, input dataset $\mathcal{X}$
Ensure: Obtain the selected tokens set S^K and update S^U in each epoch
1: **for** $t \leftarrow 1$ **to** T **do**
2:       Sample data sample from $\mathcal{X}$, feed-forwarded through the embedding to obtain the output token set S_N
3:       $s \leftarrow \frac{1}{2}(1-m)$
4:       Obtain S^I via Eq. (2) and initialize S^U
5:       Obtain the current training stage $\zeta = \lceil N_g * t/T \rceil$
6:       Calculate $distance(S^U \rightarrow S^I)_i$ for $i \in \{1, \cdots, |S^U|\}$ via Eq. (3) and Eq. (4)
7:       Obtain S^* and update S^K, S^U via Eq. (5) and Eq. (6)
8: **end for**

Table 3: Top-1 classification accuracy on RESISC-45 [77]. "-" indicates unavailable accuracy data. Training throughput was measured using 8 NVIDIA 40G A100 GPUs.

Model	Publication	Backbone	Params	Data Throughput/Min.	Acccuracy
MAE [10]	CVPR'22	ViT-B	86M	17k	93.45
CrossMAE [45]	Arxiv'24	ViT-B	86M	22k	92.82
SatMAE [30]	NIPS'22	ViT-B	86M	15k	-
ScaleMAE [33]	ICCV'23	ViT-B	86M	16k	-
SelectiveMAE	-	ViT-B	86M	**37k** (2.2×)	**94.58** (+1.13)
MAE [10]	CVPR'22	ViT-L	307M	15k	93.80
SatMAE [30]	NIPS'22	ViT-L	307M	13k	94.10
ScaleMAE [33]	ICCV'23	ViT-L	307M	13k	95.04
SelectiveMAE	-	ViT-L	307M	**41k** (2.7×)	**95.77** (+1.97)

$$S^K = S^I \cup S^*, \quad S^U = S^U \setminus S^*, \tag{6}$$

where S^* represents the selected token from S^U. The operations in Eq. (5) and Eq. (6) are performed in each training epoch. This process is summarized in Algorithm 1.

5 Experiment

In this section, we first discuss the pre-training process using the RS-4M dataset, comparing the training speed and performance of our proposed SelectiveMAE with existing MAE acceleration methods. We then demonstrate SelectiveMAE's superior performance across various downstream tasks compared to different RSFMs. Finally, we explore design choices such as the reconstruction ratio, mask ratio, and decoder depth through extensive ablation experiments, detailed in the Appendix.

5.1 Pre-training

Pre-training Setup. Our pre-training experiment setup largely follows MAE [10]. Unlike other MIM methods in the RS field, such as SatMAE [30] and ScaleMAE [33], we train both the commonly used ViT-B and the larger ViT-L backbones [39]. We adjust the input image to a size of 224×224, with a patch size of 16, using the AdamW optimizer and a cosine learning rate scheduler. The initial learning rate is set to 1.5e-4, batch size to 1024, masking ratio to 85%, and reconstruction ratio to 25%. For patch selection during the 800 epochs, the adjustment thresholds are set at 300 epochs, with the last 200 epochs using random distance to enhance robustness.

Pre-training Results.

We pre-trained ViT-B and ViT-L on the RS-4M dataset, evaluating the image data throughput per minute for SelectiveMAE and the baseline (MAE) [10]. We also assessed the training speed of the general domain acceleration method CrossMAE [45], as well as the remote sensing methods SatMAE [30] and ScaleMAE [33]. Table 3 illustrates our method's more than doubled acceleration for both base and large ViT models compared to the vanilla MAE baseline. It also outperforms the general domain acceleration method CrossMAE significantly. Additionally, we reported the top-1

Table 4: Results for scene classification, object detection, and semantic segmentation. "TR" represents the ratio of training data to the entire dataset.

Model	Publication	Backbone	Sence Classification		Object Detection		Semantic Segmentation	
			AID	RESISC-45	DIOR	DIOR-R	LoveDA	SpaceNetv1
			(TR=20%/50%)	(TR=10%/20%)	mAP_{50}	mAP_{50}	mIoU	mF1
SeCo [22]	ICCV'21	ResNet-50	93.47/95.99	89.64/92.91	-	-	43.63	77.09
GASSL [24]	ICCV'21	ResNet-50	93.55/95.92	90.86/93.06	67.40	65.65	48.76	78.51
TOV [28]	JSTARS'23	ResNet-50	95.16/97.09	90.97/93.79	70.16	66.33	49.70	-
CACo [21]	CVPR'23	ResNet-50	90.88/95.05	88.28/91.94	66.91	64.10	48.89	77.94
SatMAE [30]	NIPS'22	ViT-L	95.02/96.94	91.72/94.10	70.89	65.66	-	78.07
ScaleMAE [33]	ICCV'23	ViT-L	96.44/97.58	92.63/95.04	73.81	66.47	-	-
SSL4EO [82]	GRSM'23	ViT-S	91.06/94.74	87.60/91.27	64.82	61.23	-	-
RingMo [37]	TGRS'22	Swin-B	96.90/98.34	94.25/95.67	75.90	-	-	-
SatLas [83]	ICCV'23	Swin-B	94.96/97.38	92.16/94.70	74.10	67.59	-	-
GFM [25]	ICCV'23	Swin-B	95.47/97.09	92.73/94.64	72.84	67.67	-	-
RVSA [18]	TGRS'23	ViT-B+RVSA	97.03/**98.50**	93.93/95.69	75.80	68.06	51.95	-
SelectiveMAE	-	ViT-B	96.78/98.12	93.35/94.58	75.70	67.78	53.05	**79.50**
SelectiveMAE	-	ViT-L	**97.25**/98.48	**94.57/95.77**	**77.80**	**70.31**	**54.31**	79.46

classification accuracy on the same dataset, with both MAE and CrossMAE trained on MillionAID [20]. Table 3 clearly demonstrates our method's superior speed and performance.

The significant acceleration effect of SelectiveMAE stems from utilizing only 40% of the image patches (15% for the encoder and 25% for the decoder). Despite this reduced utilization, it achieves superior performance compared to other acceleration methods [45] due to the proposed novel token masking and reconstruction strategy, tailored for the remote sensing images. This unique approach ensures that SelectiveMAE delivers both speed and high performance, as validated in Table 4.

5.2 Fine-tuning on Downstream Tasks

We further evaluated SelectiveMAE across three key downstream tasks: scene classification, object detection, and semantic segmentation. In addition to benchmarking against MAE-based approaches like SatMAE[30], ScaleMAE[33], SSL4EO[82], RVSA [18], RingMo[37], and GFM[25], we compared it with other leading visual foundation models. These encompass methods leveraging contrastive learning and enhanced backbones, such as GASSL [24], SeCo [22], TOV [28], and CACo [21], and advanced supervised learning based approaches [83]. Notably, none of these comparative methods were specifically tailored for accelerated pre-training, and although their speed performance wasn't reported, we anticipate they may lag behind the computationally efficient baseline (MAE). To ensure fairness, all experiments followed to consistent fine-tuning settings. Supplementary materials and code provide comprehensive experimental details.

Scene Classification. We begin by evaluating the pre-trained model's performance on the scene classification task, which offers insight into its overall representation capability without requiring additional decoders. We leverage two scene classification datasets: AID [84] and RESISC-45 [77]. Training details, including the training and test split ratio, adhere to [18, 33], with further specifics available in our code. Evaluation is based on overall accuracy (OA). Table 4 presents the results, demonstrating SelectiveMAE's competitive performance compared to other pre-training methods on both datasets. Notably, our method enjoys a significantly faster training speed, *e.g.*, over $2\times$ faster than the MAE baseline.

Besides, it outperforms RVSA and others when scaled to ViT-L. This demonstrates that, with our SelectiveMAE training method on the RS-4M dataset, the model can learn strong feature representations and scale efficiently.

Horizontal & Oriented Object Detection. We utilized the well-established DIOR dataset for horizontal object detection [85] and its improved variant DIOR-R for oriented object detection [86], both comprising RGB images. Following the methodologies of previous works [18, 37], we maintained consistent experimental setups, employing Faster-RCNN [87] and Oriented-RCNN [88] as detectors for each dataset. Detailed experimental configurations are available in the accompanying code. The results are summarized in Table 4. Our approach, utilizing a ViT-B backbone, demonstrates competitive or superior performance compared to other methods with a Swin-B backbone, such as RingMo [37], SatLas [83], and GFM [25]. This is particularly noteworthy as hierarchical transformers

generally excel at generating multiscale features essential for object detection. Moreover, our SelectiveMAE with a ViT-B backbone outperforms SatMAE [30] and ScaleMAE [33], which use a larger ViT-L backbone, and matches the advanced RVSA [18, 34] that employs specialized window attention. When using the larger ViT-L backbone, SelectiveMAE shows significantly enhanced performance across both detection datasets, underscoring the excellent scalability of our method.

Semantic Segmentation. We further evaluate the performance of the pre-trained model on pixel-level perception tasks, particularly semantic segmentation, using two well-known remote sensing datasets: LoveDA [51] and SpaceNetv1 [52]. Our implementation closely follows [18], utilizing UperNet [89] as the segmentation framework, with mean Intersection over Union (mIOU) as the evaluation metric. Table 4 demonstrates the clear superiority of SelectiveMAE over its competitors in pixel-level semantic segmentation. The selection and reconstruction strategies employed by SelectiveMAE focus on semantically rich patches, such as the boundaries between foreground objects and background stuff, leading to better representation learning for segmentation.

6 Conclusion

In this paper, we introduce RS-4M, a large-scale optical remote sensing dataset for unsupervised learning. Unlike previous datasets in the RS field, RS-4M offers a significantly larger and more diverse image set with fine-grained details relevant to downstream tasks. Benchmarking representative MIM methods on RS-4M highlights its advantages in these tasks. To address the computational burden of MIM training on large-scale RS datasets, we propose SelectiveMAE, an efficient MIM method that dynamically encodes and reconstructs patch tokens based on their semantic richness. SelectiveMAE significantly accelerates training, demonstrating that only 40% of RS image patches are needed to train a comparable MIM model. Experiments show that SelectiveMAE not only achieves over $2\times$ speedup in pre-training but also enhances performance in various downstream tasks.

Limitations and Discussion. Although the RS-4M dataset surpasses existing RS datasets by more than four times, its size can be further increased by collecting and filtering additional RS data. Additionally, its diversity can be enhanced by incorporating data from various types of sensors.

References

[1] Nathalie Pettorelli, Henrike Schulte to Bühne, Ayesha Tulloch, Grégoire Dubois, Cate Macinnis-Ng, Ana M Queirós, David A Keith, Martin Wegmann, Franziska Schrodt, Marion Stellmes, et al. Satellite remote sensing of ecosystem functions: opportunities, challenges and way forward. *Remote Sensing in Ecology and Conservation*, 4(2):71–93, 2018.

[2] Olalekan Mumin Bello and Yusuf Adedoyin Aina. Satellite remote sensing as a tool in disaster management and sustainable development: towards a synergistic approach. *Procedia-Social and Behavioral Sciences*, 120:365–373, 2014.

[3] Liang Huang, Fengxiang Wang, Yalun Zhang, and Qingxia Xu. Fine-grained ship classification by combining cnn and swin transformer. *Remote Sensing*, 14(13):3087, 2022.

[4] Fengxiang Wang, Deying Yu, Liang Huang, Yalun Zhang, Yongbing Chen, and Zhiguo Wang. Fine-grained ship image classification and detection based on a vision transformer and multi-grain feature vector fpn model. *Geo-spatial Information Science*, pages 1–22, 2024.

[5] Tongdi He and Shengxin Wang. Multi-spectral remote sensing land-cover classification based on deep learning methods. *The Journal of Supercomputing*, 77(3):2829–2843, 2021.

[6] Gong Cheng, Xingxing Xie, Junwei Han, Lei Guo, and Gui-Song Xia. Remote sensing image scene classification meets deep learning: Challenges, methods, benchmarks, and opportunities. *IEEE Journal of Selected Topics in Applied Earth Observations and Remote Sensing*, 13:3735–3756, 2020.

[7] Wentong Li, Yijie Chen, Kaixuan Hu, and Jianke Zhu. Oriented reppoints for aerial object detection. In *Proceedings of the IEEE/CVF Conference on Computer Vision and Pattern Recognition (CVPR)*, pages 1829–1838, June 2022.

[8] Curtis E Woodcock, Thomas R Loveland, Martin Herold, and Marvin E Bauer. Transitioning from change detection to monitoring with remote sensing: A paradigm shift. *Remote Sensing of Environment*, 238:111558, 2020.

[9] Xiaohui Yuan, Jianfang Shi, and Lichuan Gu. A review of deep learning methods for semantic segmentation of remote sensing imagery. *Expert Systems with Applications*, 169:114417, 2021.

[10] Kaiming He, Xinlei Chen, Saining Xie, Yanghao Li, Piotr Dollár, and Ross Girshick. Masked Autoencoders Are Scalable Vision Learners. In *CVPR*, 2022.

[11] Zhenda Xie, Zheng Zhang, Yue Cao, Yutong Lin, Jianmin Bao, Zhuliang Yao, Qi Dai, and Han Hu. Simmim: A simple framework for masked image modeling. In *Proceedings of the IEEE/CVF conference on computer vision and pattern recognition*, pages 9653–9663, 2022.

[12] Yufei Xu, Jing Zhang, Qiming Zhang, and Dacheng Tao. Vitpose: Simple vision transformer baselines for human pose estimation. *Advances in Neural Information Processing Systems*, 35:38571–38584, 2022.

[13] Qiming Zhang, Yufei Xu, Jing Zhang, and Dacheng Tao. Vitaev2: Vision transformer advanced by exploring inductive bias for image recognition and beyond. *International Journal of Computer Vision*, 131(5):1141–1162, 2023.

[14] Yufei Xu, Jing Zhang, Qiming Zhang, and Dacheng Tao. Vitpose++: Vision transformer for generic body pose estimation. *IEEE Transactions on Pattern Analysis and Machine Intelligence*, 2023.

[15] Qiming Zhang, Jing Zhang, Yufei Xu, and Dacheng Tao. Vision transformer with quadrangle attention. *IEEE Transactions on Pattern Analysis and Machine Intelligence*, 2024.

[16] Fengxiang Wang, Wanrong Huang, Shaowu Yang, Qi Fan, and Long Lan. Learning to learn better visual prompts. In *Proceedings of the AAAI Conference on Artificial Intelligence*, volume 38, pages 5354–5363, 2024.

[17] Jingyi Wang, Xiaobo Xia, Long Lan, Xinghao Wu, Jun Yu, Wenjing Yang, Bo Han, and Tongliang Liu. Tackling noisy labels with network parameter additive decomposition. *IEEE Transactions on Pattern Analysis and Machine Intelligence*, 2024.

[18] Di Wang, Qiming Zhang, Yufei Xu, Jing Zhang, Bo Du, Dacheng Tao, and Liangpei Zhang. Advancing plain vision transformer toward remote sensing foundation model. *IEEE Transactions on Geoscience and Remote Sensing*, 61:1–15, 2023.

[19] Tal Ridnik, Emanuel Ben-Baruch, Asaf Noy, and Lihi Zelnik-Manor. Imagenet-21k pretraining for the masses. *arXiv preprint arXiv:2104.10972*, 2021.

[20] Yang Long, Gui-Song Xia, Shengyang Li, Wen Yang, Michael Ying Yang, Xiao Xiang Zhu, Liangpei Zhang, and Deren Li. On creating benchmark dataset for aerial image interpretation: Reviews, guidances and million-aid. *IEEE Journal of Selected Topics in Applied Earth Observations and Remote Sensing*, 14:4205–4230, 2021.

[21] Utkarsh Mall, Bharath Hariharan, and Kavita Bala. Change-aware sampling and contrastive learning for satellite images. In *Proceedings of the IEEE/CVF Conference on Computer Vision and Pattern Recognition*, pages 5261–5270, 2023.

[22] Oscar Mañas, Alexandre Lacoste, Xavier Giró-i Nieto, David Vazquez, and Pau Rodríguez. Seasonal Contrast: Unsupervised Pre-Training From Uncurated Remote Sensing Data. In *ICCV*, 2021.

[23] Gencer Sumbul, Arne de Wall, Tristan Kreuziger, Filipe Marcelino, Hugo Costa, Pedro Benevides, Mário Caetano, Begüm Demir, and Volker Markl. BigEarthNet-MM: A Large-Scale, Multimodal, Multilabel Benchmark Archive for Remote Sensing Image Classification and Retrieval [Software and Data Sets]. *IEEE Geoscience and Remote Sensing Magazine*, 2021.

[24] Kumar Ayush, Burak Uzkent, Chenlin Meng, Kumar Tanmay, Marshall Burke, David Lobell, and Stefano Ermon. Geography-Aware Self-Supervised Learning. In *ICCV*, 2021.

[25] Matías Mendieta, Boran Han, Xingjian Shi, Yi Zhu, and Chen Chen. Towards geospatial foundation models via continual pretraining. In *Proceedings of the IEEE/CVF International Conference on Computer Vision*, pages 16806–16816, 2023.

[26] Ziyue Huang, Mingming Zhang, Yuan Gong, Qingjie Liu, and Yunhong Wang. Generic knowledge boosted pre-training for remote sensing images. *IEEE Transactions on Geoscience and Remote Sensing*, 2024.

[27] Di Wang, Jing Zhang, Bo Du, Minqiang Xu, Lin Liu, Dacheng Tao, and Liangpei Zhang. SAMRS: Scaling-up remote sensing segmentation dataset with segment anything model. *Advances in Neural Information Processing Systems*, 36, 2024.

[28] Chao Tao, Ji Qi, Guo Zhang, Qing Zhu, Weipeng Lu, and Haifeng Li. Tov: The original vision model for optical remote sensing image understanding via self-supervised learning. *IEEE Journal of Selected Topics in Applied Earth Observations and Remote Sensing*, 2023.

[29] Keumgang Cha, Junghoon Seo, and Taekyung Lee. A billion-scale foundation model for remote sensing images. *arXiv preprint arXiv:2304.05215*, 2023.

[30] Yezhen Cong, Samar Khanna, Chenlin Meng, Patrick Liu, Erik Rozi, Yutong He, Marshall Burke, David Lobell, and Stefano Ermon. Satmae: Pre-training transformers for temporal and multi-spectral satellite imagery. *Advances in Neural Information Processing Systems*, 35:197–211, 2022.

[31] Fanglong Yao, Wanxuan Lu, Heming Yang, Liangyu Xu, Chenglong Liu, Leiyi Hu, Hongfeng Yu, Nayu Liu, Chubo Deng, Deke Tang, et al. Ringmo-sense: Remote sensing foundation model for spatiotemporal prediction via spatiotemporal evolution disentangling. *IEEE Transactions on Geoscience and Remote Sensing*, 2023.

[32] Wenyuan Li, Keyan Chen, and Zhenwei Shi. Geographical supervision correction for remote sensing representation learning. *IEEE Transactions on Geoscience and Remote Sensing*, 60:1–20, 2022.

[33] Colorado J. Reed, Ritwik Gupta, Shufan Li, Sarah Brockman, Christopher Funk, Brian Clipp, Kurt Keutzer, Salvatore Candido, Matt Uyttendaele, and Trevor Darrell. Scale-MAE: A Scale-Aware Masked Autoencoder for Multiscale Geospatial Representation Learning. *CoRR*, abs/2212.14532, 2023.

[34] Di Wang, Jing Zhang, Minqiang Xu, Lin Liu, Dongsheng Wang, Erzhong Gao, Chengxi Han, Haonan Guo, Bo Du, Dacheng Tao, and Liangpei Zhang. Mtp: Advancing remote sensing foundation model via multi-task pretraining. *IEEE Journal of Selected Topics in Applied Earth Observations and Remote Sensing*, pages 1–24, 2024.

[35] Maofeng Tang, Andrei Liviu Cozma, Konstantinos Georgiou, and Hairong Qi. Cross-scale mae: A tale of multiscale exploitation in remote sensing. In *Thirty-seventh Conference on Neural Information Processing Systems*, 2023.

[36] Mubashir Noman, Muzammal Naseer, Hisham Cholakkal, Rao Muhammad Anwar, Salman Khan, and Fahad Shahbaz Khan. Rethinking transformers pre-training for multi-spectral satellite imagery. In *CVPR*, 2024.

[37] Xian Sun, Peijin Wang, Wanxuan Lu, Zicong Zhu, Xiaonan Lu, Qibin He, Junxi Li, Xuee Rong, Zhujun Yang, Hao Chang, et al. Ringmo: A remote sensing foundation model with masked image modeling. *IEEE Transactions on Geoscience and Remote Sensing*, 2022.

[38] Dilxat Muhtar, Xueliang Zhang, Pengfeng Xiao, Zhenshi Li, and Feng Gu. Cmid: A unified self-supervised learning framework for remote sensing image understanding. *IEEE Transactions on Geoscience and Remote Sensing*, 61:1–17, 2023.

[39] Alexey Dosovitskiy, Lucas Beyer, Alexander Kolesnikov, Dirk Weissenborn, Xiaohua Zhai, Thomas Unterthiner, Mostafa Dehghani, Matthias Minderer, Georg Heigold, Sylvain Gelly, Jakob Uszkoreit, and Neil Houlsby. An Image is Worth 16x16 Words: Transformers for Image Recognition at Scale. In *ICLR*, 2021.

[40] Agrim Gupta, Jiajun Wu, Jia Deng, and Fei-Fei Li. Siamese masked autoencoders. *Advances in Neural Information Processing Systems*, 36, 2024.

[41] Haoqing Wang, Yehui Tang, Yunhe Wang, Jianyuan Guo, Zhi-Hong Deng, and Kai Han. Masked image modeling with local multi-scale reconstruction. In *Proceedings of the IEEE/CVF Conference on Computer Vision and Pattern Recognition*, pages 2122–2131, 2023.

[42] Jin Li, Yaoming Wang, Xiaopeng Zhang, Yabo Chen, Dongsheng Jiang, Wenrui Dai, Chenglin Li, Hongkai Xiong, and Qi Tian. Progressively compressed auto-encoder for self-supervised representation learning. In *The Eleventh International Conference on Learning Representations*, 2022.

[43] Jun Chen, Ming Hu, Boyang Li, and Mohamed Elhoseiny. Efficient self-supervised vision pretraining with local masked reconstruction. *arXiv preprint arXiv:2206.00790*, 2022.

[44] Jianyuan Guo, Kai Han, Han Wu, Yehui Tang, Yunhe Wang, and Chang Xu. Fastmim: Expediting masked image modeling pre-training for vision. *arXiv preprint arXiv:2212.06593*, 2022.

[45] Letian Fu, Long Lian, Renhao Wang, Baifeng Shi, Xudong Wang, Adam Yala, Trevor Darrell, Alexei A Efros, and Ken Goldberg. Rethinking patch dependence for masked autoencoders. *arXiv preprint arXiv:2401.14391*, 2024.

[46] Ben G Weinstein, Sergio Marconi, Stephanie A Bohlman, Alina Zare, Aditya Singh, Sarah J Graves, and Ethan P White. A remote sensing derived data set of 100 million individual tree crowns for the national ecological observatory network. *Elife*, 10:e62922, 2021.

[47] Gordon Christie, Neil Fendley, James Wilson, and Ryan Mukherjee. Functional map of the world. In *Proceedings of the IEEE Conference on Computer Vision and Pattern Recognition*, pages 6172–6180, 2018.

[48] Jan Gasienica-Jozkowy, Mateusz Knapik, and Bogusław Cyganek. An ensemble deep learning method with optimized weights for drone-based water rescue and surveillance. *Integrated Computer-Aided Engineering*, 28(3):221–235, 2021.

[49] Long Lan, Fengxiang Wang, Shuyan Li, Xiangtao Zheng, Zengmao Wang, and Xinwang Liu. Efficient prompt tuning of large vision-language model for fine-grained ship classification. *arXiv preprint arXiv:2403.08271*, 2024.

[50] Gaetan Bahl, Mehdi Bahri, and Florent Lafarge. Single-shot end-to-end road graph extraction. In *Proceedings of the IEEE/CVF Conference on Computer Vision and Pattern Recognition*, pages 1403–1412, 2022.

[51] Junjue Wang, Zhuo Zheng, Ailong Ma, Xiaoyan Lu, and Yanfei Zhong. LoveDA: A remote sensing land-cover dataset for domain adaptive semantic segmentation. In *NeurIPS Track on Datasets and Benchmarks*, volume 1, 2021.

[52] Adam Van Etten, Dave Lindenbaum, and Todd M Bacastow. Spacenet: A remote sensing dataset and challenge series. *arXiv preprint arXiv:1807.01232*, 2018.

[53] Michael Schmitt, Lloyd Haydn Hughes, Chunping Qiu, and Xiao Xiang Zhu. Sen12ms–a curated dataset of georeferenced multi-spectral sentinel-1/2 imagery for deep learning and data fusion. *arXiv preprint arXiv:1906.07789*, 2019.

[54] Di Wang, Jing Zhang, Bo Du, Gui-Song Xia, and Dacheng Tao. An empirical study of remote sensing pretraining. *IEEE Transactions on Geoscience and Remote Sensing*, 61:1–20, 2023.

[55] Xinye Wanyan, Sachith Seneviratne, Shuchang Shen, and Michael Kirley. Dino-mc: Self-supervised contrastive learning for remote sensing imagery with multi-sized local crops. *arXiv preprint arXiv:2303.06670*, 2023.

[56] Jeremy Irvin, Lucas Tao, Joanne Zhou, Yuntao Ma, Langston Nashold, Benjamin Liu, and Andrew Y Ng. Usat: A unified self-supervised encoder for multi-sensor satellite imagery. *arXiv preprint arXiv:2312.02199*, 2023.

[57] Xin Guo, Jiangwei Lao, Bo Dang, Yingying Zhang, Lei Yu, Lixiang Ru, Liheng Zhong, Ziyuan Huang, Kang Wu, Dingxiang Hu, et al. Skysense: A multi-modal remote sensing foundation model towards universal interpretation for earth observation imagery. *arXiv preprint arXiv:2312.10115*, 2023.

[58] Boran Han, Shuai Zhang, Xingjian Shi, and Markus Reichstein. Bridging remote sensors with multisensor geospatial foundation models. *arXiv preprint arXiv:2404.01260*, 2024.

[59] Nikolaos Ioannis Bountos, Arthur Ouaknine, and David Rolnick. Fomo-bench: a multi-modal, multi-scale and multi-task forest monitoring benchmark for remote sensing foundation models. *arXiv preprint arXiv:2312.10114*, 2023.

[60] Danfeng Hong, Bing Zhang, Xuyang Li, Yuxuan Li, Chenyu Li, Jing Yao, Pedram Ghamisi, Naoto Yokoya, Hao Li, Xiuping Jia, Antonio Plaza, et al. Spectralgpt: Spectral remote sensing foundation model. *IEEE Transactions on Pattern Analysis and Machine Intelligence*, 2024. DOI:10.1109/TPAMI.2024.3362475.

[61] Tom Brown, Benjamin Mann, Nick Ryder, Melanie Subbiah, Jared D Kaplan, Prafulla Dhariwal, Arvind Neelakantan, Pranav Shyam, Girish Sastry, Amanda Askell, et al. Language models are few-shot learners. *Advances in neural information processing systems*, 33:1877–1901, 2020.

[62] Mark Chen, Alec Radford, Rewon Child, Jeffrey Wu, Heewoo Jun, David Luan, and Ilya Sutskever. Generative pretraining from pixels. In *International conference on machine learning*, pages 1691–1703. PMLR, 2020.

[63] Xiao Teng, Long Lan, Jing Zhao, Xueqiong Li, and Yuhua Tang. Highly efficient active learning with tracklet-aware co-cooperative annotators for person re-identification. *IEEE Transactions on Neural Networks and Learning Systems*, 2023.

[64] Long Lan, Xiao Teng, Jing Zhang, Xiang Zhang, and Dacheng Tao. Learning to purification for unsupervised person re-identification. *IEEE Transactions on Image Processing*, 2023.

[65] Kaiming He, Xinlei Chen, Saining Xie, Yanghao Li, Piotr Dollár, and Ross Girshick. Masked autoencoders are scalable vision learners. In *Proceedings of the IEEE/CVF conference on computer vision and pattern recognition*, pages 16000–16009, 2022.

[66] Hangbo Bao, Li Dong, Songhao Piao, and Furu Wei. Beit: Bert pre-training of image transformers. In *International Conference on Learning Representations*, 2021.

[67] Chen Wei, Haoqi Fan, Saining Xie, Chao-Yuan Wu, Alan Yuille, and Christoph Feichtenhofer. Masked feature prediction for self-supervised visual pre-training. In *Proceedings of the IEEE/CVF Conference on Computer Vision and Pattern Recognition*, pages 14668–14678, 2022.

[68] Jinghao Zhou, Chen Wei, Huiyu Wang, Wei Shen, Cihang Xie, Alan Yuille, and Tao Kong. Image bert pre-training with online tokenizer. In *International Conference on Learning Representations*, 2021.

[69] Hao Liu, Xinghua Jiang, Xin Li, Antai Guo, Yiqing Hu, Deqiang Jiang, and Bo Ren. The devil is in the frequency: Geminated gestalt autoencoder for self-supervised visual pre-training. In *Proceedings of the AAAI Conference on Artificial Intelligence*, volume 37, pages 1649–1656, 2023.

[70] Yuge Shi, N Siddharth, Philip Torr, and Adam R Kosiorek. Adversarial masking for self-supervised learning. In *International Conference on Machine Learning*, pages 20026–20040. PMLR, 2022.

[71] Gang Li, Heliang Zheng, Daqing Liu, Chaoyue Wang, Bing Su, and Changwen Zheng. Semmae: Semantic-guided masking for learning masked autoencoders. *Advances in Neural Information Processing Systems*, 35:14290–14302, 2022.

[72] Shubham Tulsiani and Abhinav Gupta. Pixeltransformer: Sample conditioned signal generation. In *International Conference on Machine Learning*, pages 10455–10464. PMLR, 2021.

[73] Chen Wei, Karttikeya Mangalam, Po-Yao Huang, Yanghao Li, Haoqi Fan, Hu Xu, Huiyu Wang, Cihang Xie, Alan Yuille, and Christoph Feichtenhofer. Diffusion models as masked autoencoders. In *Proceedings of the IEEE/CVF International Conference on Computer Vision*, pages 16284–16294, 2023.

[74] Zhaowen Li, Zhiyang Chen, Fan Yang, Wei Li, Yousong Zhu, Chaoyang Zhao, Rui Deng, Liwei Wu, Rui Zhao, Ming Tang, et al. Mst: Masked self-supervised transformer for visual representation. *Advances in Neural Information Processing Systems*, 34:13165–13176, 2021.

[75] Ioannis Kakogeorgiou, Spyros Gidaris, Bill Psomas, Yannis Avrithis, Andrei Bursuc, Konstanti-nos Karantzalos, and Nikos Komodakis. What to hide from your students: Attention-guided masked image modeling. In *European Conference on Computer Vision*, pages 300–318. Springer, 2022.

[76] Chuan Qin, Meihui Sun, and Chin-Chen Chang. Perceptual hashing for color images based on hybrid extraction of structural features. *Signal processing*, 142:194–205, 2018.

[77] Gong Cheng, Junwei Han, and Xiaoqiang Lu. Remote sensing image scene classification: Benchmark and state of the art. *Proceedings of the IEEE*, 105(10):1865–1883, 2017.

[78] Wele Gedara Chaminda Bandara, Naman Patel, Ali Gholami, Mehdi Nikkhah, Motilal Agrawal, and Vishal M Patel. Adamae: Adaptive masking for efficient spatiotemporal learning with masked autoencoders. In *Proceedings of the IEEE/CVF Conference on Computer Vision and Pattern Recognition*, pages 14507–14517, 2023.

[79] Xin Wang, Yudong Chen, and Wenwu Zhu. A survey on curriculum learning. *IEEE transactions on pattern analysis and machine intelligence*, 44(9):4555–4576, 2021.

[80] Yoshua Bengio, Jérôme Louradour, Ronan Collobert, and Jason Weston. Curriculum learning. In *Proceedings of the 26th annual international conference on machine learning*, pages 41–48, 2009.

[81] Guy Hacohen and Daphna Weinshall. On the power of curriculum learning in training deep networks. In *International conference on machine learning*, pages 2535–2544. PMLR, 2019.

[82] Yi Wang, Nassim Ait Ali Braham, Zhitong Xiong, Chenying Liu, Conrad M Albrecht, and Xiao Xiang Zhu. SSL4EO-S12: A Large-Scale Multi-Modal, Multi-Temporal Dataset for Self-Supervised Learning in Earth Observation. *CoRR*, abs/2211.07044, 2022.

[83] Favyen Bastani, Piper Wolters, Ritwik Gupta, Joe Ferdinando, and Aniruddha Kembhavi. Satlaspretrain: A large-scale dataset for remote sensing image understanding. In *Proceedings of the IEEE/CVF International Conference on Computer Vision*, pages 16772–16782, 2023.

[84] Gui-Song Xia, Jingwen Hu, Fan Hu, Baoguang Shi, Xiang Bai, Yanfei Zhong, Liangpei Zhang, and Xiaoqiang Lu. Aid: A benchmark data set for performance evaluation of aerial scene classification. *IEEE Transactions on Geoscience and Remote Sensing*, 55(7):3965–3981, 2017.

[85] Ke Li, Gang Wan, Gong Cheng, Liqiu Meng, and Junwei Han. Object detection in optical remote sensing images: A survey and a new benchmark. *ISPRS journal of photogrammetry and remote sensing*, 159:296–307, 2020.

[86] Gong Cheng, Jiabao Wang, Ke Li, Xingxing Xie, Chunbo Lang, Yanqing Yao, and Junwei Han. Anchor-free oriented proposal generator for object detection. *IEEE Transactions on Geoscience and Remote Sensing*, 60:1–11, 2022.

[87] Shaoqing Ren, Kaiming He, Ross Girshick, and Jian Sun. Faster r-cnn: Towards real-time object detection with region proposal networks. *IEEE Transactions on Pattern Analysis and Machine Intelligence*, 39(6):1137–1149, 2017.

[88] Xingxing Xie, Gong Cheng, Jiabao Wang, Xiwen Yao, and Junwei Han. Oriented r-cnn for object detection. In *Proceedings of the IEEE/CVF International Conference on Computer Vision (ICCV)*, pages 3520–3529, October 2021.

[89] Tete Xiao, Yingcheng Liu, Bolei Zhou, Yuning Jiang, and Jian Sun. Unified perceptual parsing for scene understanding. In *Proceedings of the European conference on computer vision (ECCV)*, pages 418–434, 2018.

[90] Timnit Gebru, Jamie Morgenstern, Briana Vecchione, Jennifer Wortman Vaughan, Hanna Wallach, Hal Daumé Iii, and Kate Crawford. Datasheets for datasets. *Communications of the ACM*, 64(12):86–92, 2021.

7 Overview of the Appendix

This technical appendix provides additional details of the proposed **SelectiveMAE** and **RS-4M**, as well as experimental results that are omitted from the main body of this paper due to the page limit.

Specifically, this appendix is organized as follows:

- Sec. 7.1 offers additional experimental results for the RS-4M dataset.
- Sec. 7.2 provides a detailed ablation study of SelectiveMAE.
- Sec. 7.3 provides the full experiment configurations of pretraining and downstream tasks.
- Sec. 7.4 visualizes the samples of RS-4M and predicted results of SelectiveMAE on the downstream tasks.
- Sec. 7.5 offers the Datasheets for the RS-4M dataset.
- Sec. 7.6 offers the Limitation and Potential Societal Impact.

7.1 More results on the RS-4M

For the RS-4M dataset, we further validated several downstream tasks discussed earlier in the main text, such as object detection and semantic segmentation. Specifically, we assessed the effectiveness of RS-4M compared to MillionAID [20] with equivalent data throughput using MAE [10].

Table 5: Comparison of downstream task performance at matched data throughput between Million-AID and RS-4M, assessed using MAE pre-training.

Dataset	Method	Images Number	Epoch	Sence Classification		Object Detection		Semantic Segmentation	
				AID	RESISC-45	DIOR	DIOR-R	LoveDA	SpaceNetv1
				OA (TR=20% / 50%)	OA (TR=10% / 20%)	mAP_{50}	mAP_{50}	mIoU	mF1
MillionAID	MAE	1 million	800	94.92/97.38	89.20/93.60	71.80	62.33	51.24	79.24
RS-4M	MAE	2 million	400	96.64/98.10	91.80/94.31	73.90	65.95	52.86	79.37
RS-4M	MAE	3 million	267	**96.67/98.18**	92.24/**94.41**	**75.40**	**67.07**	52.39	**79.37**
RS-4M	MAE	4 million	200	96.10/98.03	**92.38**/94.30	74.70	66.26	**52.75**	79.23

Table 5 demonstrates that our proposed RS-4M significantly enhances performance across various downstream tasks under equivalent data throughput. Particularly in practical applications like object detection and segmentation, RS-4M exhibits distinct advantages. As data volume increases, models pre-trained on RS-4M consistently outperform others across these tasks. However, it is noteworthy that performance ceases to improve once the data volume exceeds 4 million points. We attribute the initial performance gains, up to 3 million data points, to effective training where additional data volume enhances efficacy. Beyond 4 million points, the model may not achieve full optimization within 200 epochs, thus limiting comprehensive performance benefits.

In summary, Table 5 underscores the diversity of RS-4M and highlights the influence of both data volume and training epochs on pre-training models. This emphasizes the importance of adequate training on large datasets. To further exploit the potential of RS-4M, we conducted extended training using the MAE pre-training method and ViT-B, maintaining consistent settings while varying the number of training epochs. Table 6 presents the corresponding fine-tuning performance.

Table 6: Performance on downstream tasks using MAE pre-trained models with different epochs on RS-4M.

Dataset	Method	Images Number	Epoch	Sence Classification		Object Detection		Semantic Segmentation	
				AID	RESISC-45	DIOR	DIOR-R	LoveDA	SpaceNetv1
				OA (TR=20% / 50%)	OA (TR=10% / 20%)	mAP_{50}	mAP_{50}	mIoU	mF1
RS-4M	MAE	3 million	267	96.67/98.18	92.24/94.41	75.40	67.07	52.39	79.37
RS-4M	MAE	4 million	100	95.12/97.54	91.26/93.85	-	-	-	-
RS-4M	MAE	4 million	200	96.10/98.03	92.38/94.30	74.70	66.26	52.75	79.23
RS-4M	MAE	4 million	400	96.36/98.16	92.41/94.03	-	-	-	-
RS-4M	MAE	4 million	800	**96.88/98.22**	**92.44/94.43**	**75.40**	**67.35**	**52.80**	**79.41**

16

From Table 6, it is evident that as the number of epochs increases, RS-4M demonstrates increasingly significant advantages in downstream tasks. This suggests that RS-4M requires extended training to fully leverage its capabilities. However, we observe diminishing returns in performance improvement with additional epochs. This indicates that adjusting epochs alone may not fully exploit RS-4M's potential. Exploring more effective pre-training techniques, such as the proposed SelectiveMAE, could be essential for maximizing RS-4M's pre-training performance.

7.2 Ablation study of SelectiveMAE

In this section, we conducted several experiments. We first applied the MAE method to the RS-4M dataset using identical settings to those of SelectiveMAE. We then compared these results with SelectiveMAE to highlight the superiority of our proposed approach, as summarized in Table 7. Next, we conducted ablation experiments to determine the best design choice for SelectiveMAE. The results of these experiments are presented in Table 8.

Table 7: Comparison of SelectiveMAE and MAE. Results for downstream tasks under same parameter settings on RS-4M.

Method	Dataset	Epoch	Data Throu. /Min.	Sence Classification		Object Detection		Semantic Segmentation	
				AID	RESISC-45	DIOR	DIOR-R	LoveDA	SpaceNetv1
				OA (TR=20% / 50%)	OA (TR=10% / 20%)	mAP_{50}	mAP_{50}	mIoU	mF1
MAE	RS-4M	800	17k	**96.88/98.22**	92.44/94.43	75.40	67.35	52.80	79.41
SelectiveMAE	RS-4M	800	37k (2.2×)	96.78/98.12	**93.35/94.58**	**75.70**	**67.78**	**53.05**	**79.50**

Comparison of SelectiveMAE and MAE. Table 7 presents results using ViT-B as the backbone, maintaining consistent settings while varying pre-training methods. Our method achieves a **2.2×** speedup with stable improvements across most downstream tasks, particularly in detection and segmentation. In certain classification datasets like AID, there is a slight performance drop compared to MAE, with accuracy reductions not exceeding 0.1. This was expected given that the model's performance is near saturation on this dataset. SelectiveMAE accelerates by learning and reconstructing a small portion of image patches, resulting in some loss of global context. Consequently, it shows limited enhancement in tasks like scene classification, which heavily rely on overall image content. In contrast, selecting informative patches benefits downstream tasks such as Object Detection and Semantic Segmentation, where SelectiveMAE demonstrates notable gains in both speed and accuracy.

Reco. Ratio	Data Throu./Min.	AID	RESISC-45
		OA (TR=20% / 50%)	OA (TR=10% / 20%)
15%	38k	94.80/96.97	90.24/93.55
25%	**37k**	**95.41/97.92**	**91.32/94.12**

(a) **Reconstruction ratio**.

Deocder Depth	AID	RESISC-45
	OA (TR=20% / 50%)	OA (TR=10% / 20%)
4	95.16/97.58	91.03/93.84
12	**95.41/97.92**	**91.32/94.12**

(b) **Decoder depth**.

Mask ratio	Data Throu./Min.	AID	RESISC-45
		OA (TR=20% / 50%)	OA (TR=10% / 20%)
75%	29k	**96.15/98.08**	**92.48/94.63**
85%	37k	95.41/97.92	91.32/94.12

(c) **Mask ratio**.

Selection Strategy	AID	RESISC-45
	OA (TR=20% / 50%)	OA (TR=10% / 20%)
far-near-random	93.24/96.18	88.41/92.10
near-far-random	**95.41/97.92**	**91.32/94.12**

(d) **Selection strategy in PSTS**.

Table 8: Ablation study on the design choices of SelectiveMAE with ViT-B backbone pre-trained on MillionAID for 1,600 epochs. We report the top-1 fine-tuning accuracy (%) on the RESISC-45. The default settings of SelectiveMAE are highlighted in grey.

Table 8 summarizes the ablation experiments investigating various design choices of the proposed SelectiveMAE method, including Reconstruction Ratio, Mask Ratio, Decoder Depth, and the selection strategy in PSTS.

(a) Reconstruction Ratio. We explored different reconstruction ratios for SelectiveMAE. Reducing the reconstruction ratio to 15% resulted in significant performance degradation in downstream tasks. We found that a 25% reconstruction ratio strikes a balance between speed and performance in SelectiveMAE.

(b) Decoder Depth. Decreasing the number of decoder layers notably reduced performance. Given SelectiveMAE's emphasis on patch selection, we maintained 12 decoder layers without modification, providing a stable baseline for future enhancements.

(c) Mask Ratio. Adjusting the mask ratio affected the number of input patches to the encoder and thus performance. A lower mask ratio improved performance by increasing the input patches, whereas a higher ratio accelerated processing, particularly with larger encoders. In our experiments, using ViT-L yielded a **2.7**$\times$ acceleration compared to **2.2**$\times$ with ViT-B, attributable to a higher mask ratio. Hence, an 85% mask ratio was identified as the optimal balance between speed and accuracy.

(d) Selection Strategy in Progressive Semantic Token Selection (PSTS). In SelectiveMAE, PSTS begins by learning tokens that are close in distance, which provides consistent and easier patches for reconstruction. As training progresses, PSTS moves on to tokens that are farther apart, offering complementary and more challenging samples. Finally, PSTS randomly selects tokens based on distance to enhance model robustness. When we changed the selection strategy to far-near-random, training was hampered by frequent gradient explosions during pre-training. To mitigate this, we reduced the learning rate to 3e-5 (one-fifth of the original) and the batch size to 512. Although these adjustments allowed us to complete the far-near-random training, performance significantly declined.

While we have explored various design choices for SelectiveMAE, we believe its potential as a baseline method warrants further investigation. Future work may unlock greater improvements in both speed and accuracy.

7.3 Configurations of Pre-training and Fine-tuning

This section presents the datasets and implementation details for both pre-training and fine-tuning.

Pre-training: The default settings, detailed in Table 9 (i), follow the official MAE implementation. We scale the learning rate according to the ratio of the mask ratio (m) to the reconstruction ratio (r) to match the loss variance of MAE. We use 12 decoder blocks with an 85% mask ratio and a 25% reconstruction ratio. For the 800-epoch experiments, the warm-up period is adjusted to 60 epochs. All other hyperparameters remain the same as in MAE.

Scene Classification. We conducted scene classification experiments using a standard linear classifier on two commonly used datasets: AID and NWPU-RESISC45. Implementation details are summarized in Table 9 (ii).

1) *AID.* This dataset contains 10,000 images, each sized 600×600 pixels with a Ground Sample Distance (GSD) ranging from 0.5 to 8 meters. The images are categorized into 30 classes, each with approximately 220 to 400 images. We follow standard protocols in RVSA [18], using $x\%$ of the data for training and the remaining $(1-x)\%$ for testing, where $x \in \{20, 50\}$.

2) *NWPU-RESISC45 (RESISC-45).* This dataset comprises 31,500 images, each sized 256×256 pixels with a GSD ranging from 0.5 to 30 meters. It is divided into 45 categories, each containing 700 images. We use two settings, *i.e.*, 10% (and 20%) of the data for training, with the remaining 90% (and 80%) for testing, in line with previous works.

Semantic Segmentation. Semantic segmentation is extensively studied in remote sensing, which aims to automate the extraction of land use classes and ground instances. For this experiment, considering factors such as spatial resolution, spectrum, and the number of categories, we chose two well-known datasets:

1) *LoveDA.* This dataset includes urban and rural scenes with 0.3m resolution imagery from Google Earth, captured in July 2016, covering 536.15 km² across Nanjing, Changzhou, and Wuhan. It consists of 5,987 images, each 1,024×1,024 pixels, and includes seven common land cover types. We combined the official training and validation sets for training and used the official testing set for evaluation, following the common practice.

2) *SpaceNetv1.* Provided by the SpaceNet Challenge, this dataset is intended for extracting building footprints. It includes DigitalGlobe WorldView-2 satellite imagery with a 0.5m GSD, captured from 2011 to 2014, covering approximately 2,544 km² over Rio de Janeiro. It contains 382,534 building instances. We used the 6,940 images from the original training set, randomly splitting them into 5,000 images for training and the remainder for testing, in line with previous studies.

Task	(i) Pre-training	(ii) Scene Classification	
Dataset	RS-4M	AID	RESISC-45
Optimizer	AdamW	AdamW	AdamW
Input Size	224×224	224×224	224×224
Input channel	RGB	RGB	RGB
Base learning rate	1.5e-4	1e-3	1e-3
Learning rate scheduler	Cosine Annealing	Cosine Annealing	Cosine Annealing
Weight decay	0.05	0.05	0.05
Optimizer momentum	(0.9, 0.95)	(0.9, 0.999)	(0.9, 0.999)
Batch size	1024	64	64
Max iteration/epoch	800 epoch	200 epoch	200 epoch
Warmup	linear	linear	linear
Warmup iteration/epoch	60 epoch	5 epoch	5 epoch
Drop path rate	-	0.1	0.1
Augmentation	RandoCrop, RandomFlip	RandomCrop, RandomErasing	RandomCrop, RandomErasing
Head/Detector	-	Linear Classifier	Linear Classifier
Loss function	-	CrossEntropy	CrossEntropy

Task	(iii) Semantic Segmentation		(iv) Object Detection	
Dataset	LoveDA	SpaceNetv1	DIOR	DIOR-R
Optimizer	AdamW	AdamW	AdamW	AdamW
Input Size	512 × 512	384 × 384	800×800	800×800
Input channel	RGB	RGB	RGB	RGB
Base learning rate	6e-5	6e-5	1e-4	1e-4
Learning rate scheduler	Cosine Annealing	Cosine Annealing	Multistep	Multistep
Weight decay	0.05	0.05	0.05	0.05
Batch size	8	8	4	4
Max iteration/epoch	80k iters	80k iters	12 epoch	12 epoch
Warmup	linear	linear	linear	linear
Warmup iteration/epoch	1.5k iters	1.5k iters	0.5k Iters	0.5k iters
Warmup ratio	1e-6	1e-6	1e-6	1e-6
Drop path rate	0.1	0.1	0.1	0.1
Augmentation	RandomScaling (0.5 to 2.0), RandomCrop, RandomFlip	RandomScaling (0.5 to 2.0), RandomCrop, RandomFlip	RandomFlip	RandomFlip
Head/Detector	UperNet	UperNet	Faster-RCNN	Oriented-RCNN
Loss function	CrossEntropy	CrossEntropy	CrossEntropy, L1	CrossEntropy, SmoothL1

Table 9: Detailed configurations of pre-training and fine-tuning.

We utilized UperNet as the segmentation head based on MMSegmentation[2], as described in [18, 34]. Detailed fine-tuning settings are provided in Table 9 (iii).

Horizontal & Oriented Objection Detection. We use the DIOR dataset to assess the performance of SelectiveMAE and other RSFMs in horizontal object detection tasks. Following RVSA [18], we employ Faster-RCNN as the detector, as detailed in Table 9 (iv).

1) *DIOR.* This dataset consists of 23,463 visible remote sensing images with 192,472 object instances, annotated with horizontal bounding boxes across 20 common object classes. Each image of size 800×800 has a GSD ranging from 0.5 to 30 meters. The dataset is split into 5,862 training patches, 5,863 validation patches, and 11,738 test patches. Following RVSA [18], we merge the training and validation sets for training, using the test set for evaluation. The high inter-class similarity and intra-class diversity pose significant challenges for precise localization and classification.

Remote sensing images include diverse objects such as buildings, vehicles, and bridges, which are densely distributed and vary in size, scale, and orientation. This makes object detection particularly challenging, especially for oriented object detection. To evaluate RSFMs on this task, we use the DIOR-R dataset and Oriented-RCNN as the detector, as detailed in Table 9 (iv).

2) *DIOR-R.* This dataset uses the same images as DIOR but includes oriented bounding boxes, making it suitable for oriented object detection. Following RVSA [18], we combine the training and validation sets for training, using the test set for evaluation.

For horizontal object detection and oriented object detection, we use MMDetection[3] and MMRotate[4] for implementation, respectively.

7.4 Qualitative Results

7.4.1 Visualization of RS-4M Samples.

RS-4M offers a significantly larger and more diverse image set compared to previous datasets. Specially, RS-4M encompasses a wide range of diverse RS scenarios encountered in downstream tasks such as object-level detection and pixel-level segmentation. Meanwhile, the diverse data contained in RS-4M also provides finer grained detail information to support various downstream tasks.

We selected images from the RS-4M dataset, as displayed in Figure 4. It can be seen that, RS-4M encompasses a wide range of diverse RS scenarios and provides finer grained detail information to support various downstream tasks. Nonetheless, we also find that optical remote sensing images contain numerous redundant background pixels, and the high-value information in these images often occupies only a small portion of the total pixel, a characteristic particularly evident in downstream tasks like identifying ships or bridges in satellite images.

7.4.2 Visualization of SelectiveMAE Results on Downstream Tasks

Figures 5-8 present the results of our SelectiveMAE on the DIOR, DIOR-R, LoveDA, and SpaceNetv1 datasets. We utilized the ViT-L pre-trained on RS-4M as the backbone. The results closely match the ground truth, ensuring high accuracy. For detection tasks, our methods accurately identify diverse objects of various sizes. In segmentation tasks, they facilitate extensive extraction and mapping of significant RS land cover categories. In summary, RS-4M and SelectiveMAE enable the successful construction of effective RS foundation models.

7.5 Datasheets

In this section, we follow the NeurIPS Dataset and Benchmark guideline and use the template from Gebru *et al.* [90] to document necessary information about the proposed datasets and benchmarks.

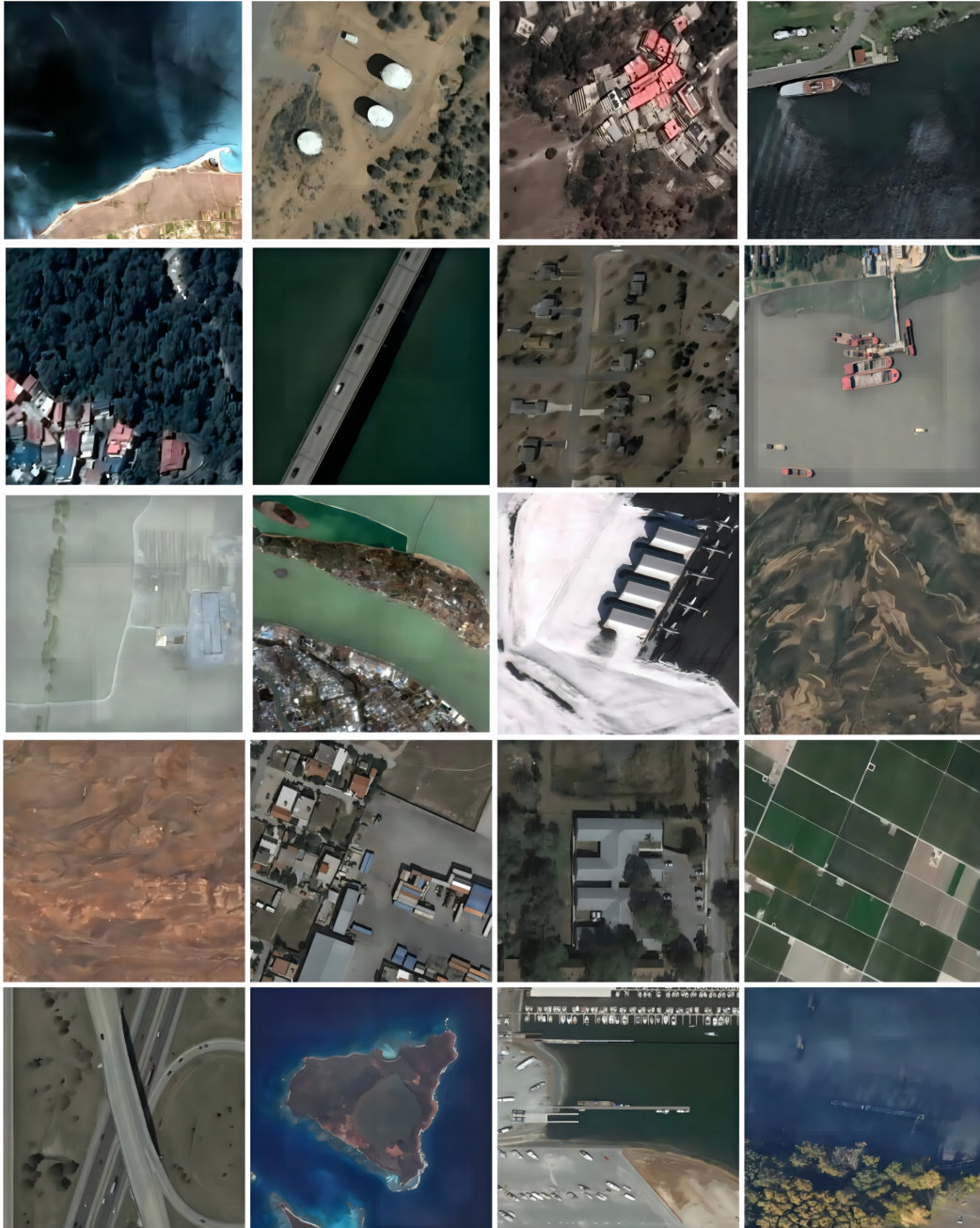[2]https://github.com/open-mmlab/mmsegmentation
[3]https://github.com/open-mmlab/mmdetection
[4]https://github.com/open-mmlab/mmrotate

Figure 4: Visualization of RS-4M Samples.

7.5.1 Motivation

The questions in this section are primarily intended to encourage dataset creators to clearly articulate their reasons for creating the dataset and to promote transparency about funding interests. The latter may be particularly relevant for datasets created for research purposes.

1. *"For what purpose was the dataset created?"*

   A: The dataset was created to support research on remote sensing foundation models (RSFMs) using self-supervised learning techniques.

2. *"Who created the dataset (e.g., which team, research group) and on behalf of which entity?"*
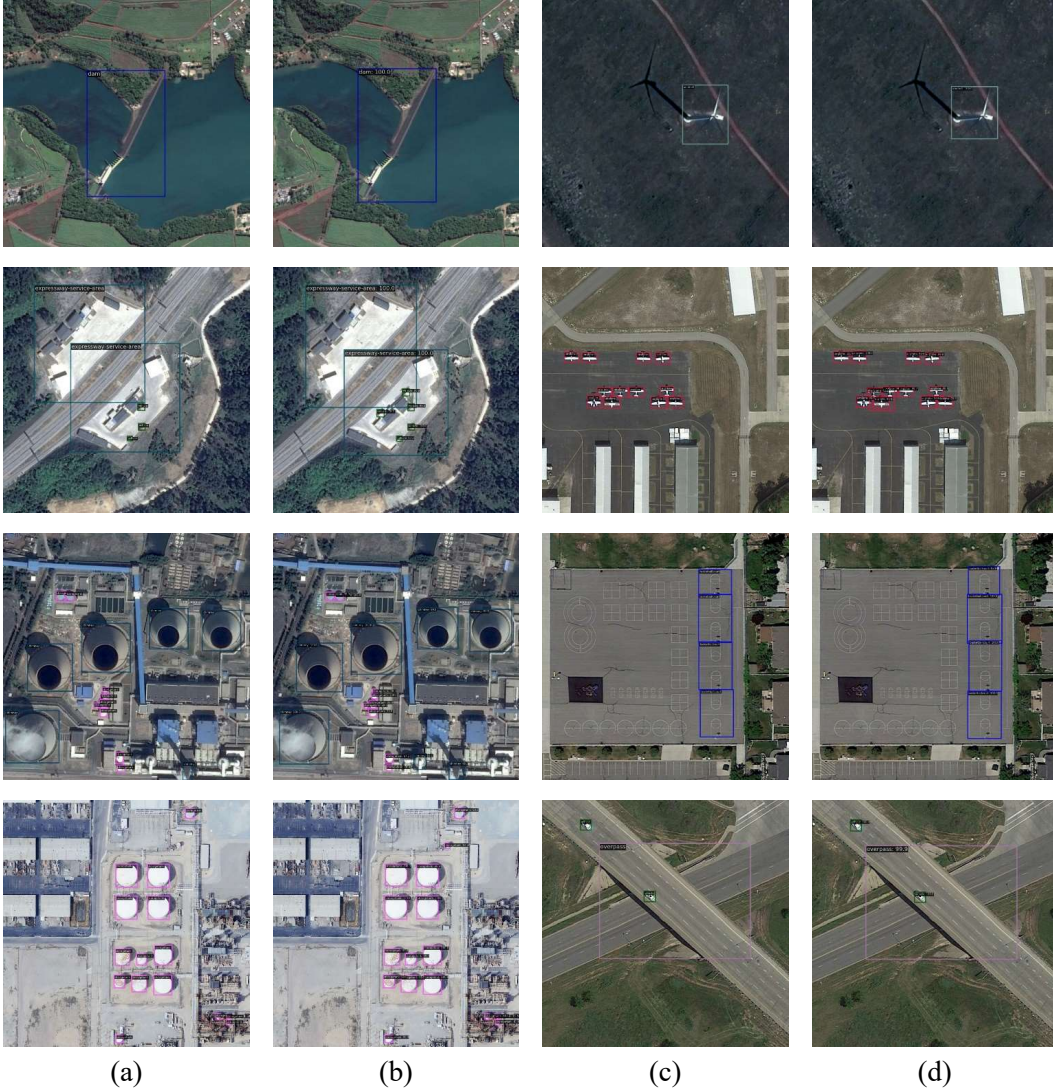
Figure 5: Visualization of SelectiveMAE predictions on the DIOR testing set. (a)(c) Ground truth. (b)(d) Predicted results of SelectiveMAE.

A: The dataset was created by:
- Fengxiang Wang (National University of Defense Technology),
- Hongzhen Wang (Tsinghua University),
- Di Wang (Wuhan University),
- Zonghao Guo (University of Chinese Academic of Sciences),
- Zhenyu Zhong (Nankai University),
- Long Lan (National University of Defense Technology),
- Jing Zhang (The University of Sydney),
- Zhiyuan Liu (Tsinghua University),
- Maosong Sun (Tsinghua University).

3. *"Who funded the creation of the dataset?"*

A: The dataset creation was funded by the affiliations of the authors involved in this work.

7.5.2 Composition

Most of the questions in this section are intended to provide dataset consumers with the information they need to make informed decisions about using the dataset for their chosen tasks. Some of the
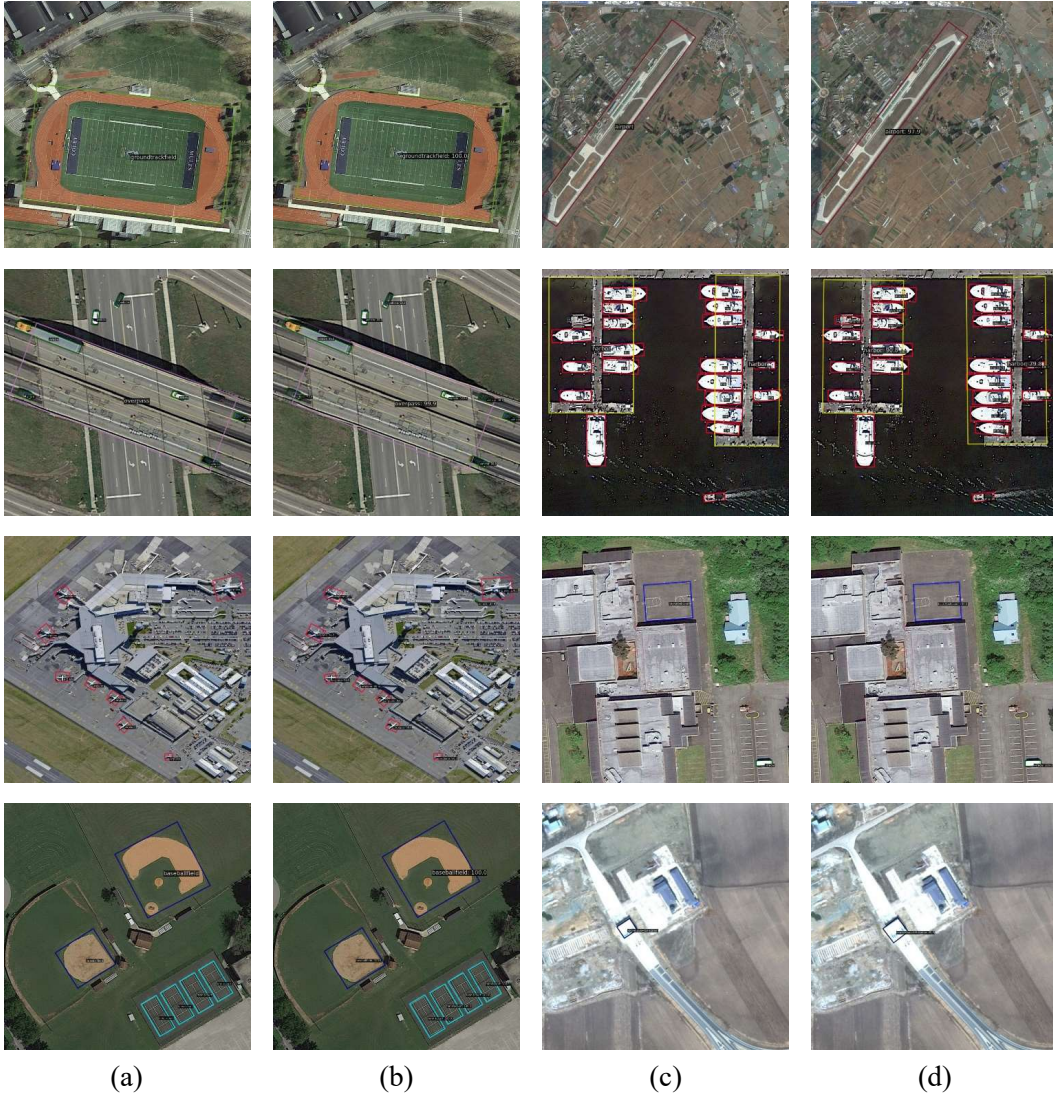
Figure 6: Visualization of SelectiveMAE predictions on the DIOR-R testing set. (a)(c) Ground truth. (b)(d) Predicted results of SelectiveMAE.

questions are designed to elicit information about compliance with the EU's General Data Protection Regulation (GDPR) or comparable regulations in other jurisdictions. Questions that apply only to datasets that relate to people are grouped together at the end of the section. We recommend taking a broad interpretation of whether a dataset relates to people. For example, any dataset containing text that was written by people relates to people.

1. *"What do the instances that comprise our datasets represent (e.g., documents, photos, people, countries)?"*
   A: The dataset primarily comprises visible light remote sensing images captured by satellites. All datasets utilized in RS-4M are publicly accessible and nonprofit.

2. *"How many instances are there in total (of each type, if appropriate)?"*
   A: RS-4M contains 4 million remote sensing image instances captured by satellites.

3. *"Does the dataset contain all possible instances or is it a sample (not necessarily random) of instances from a larger set?"*
   A: Yes, our dataset contains all possible instances that have been collected so far.

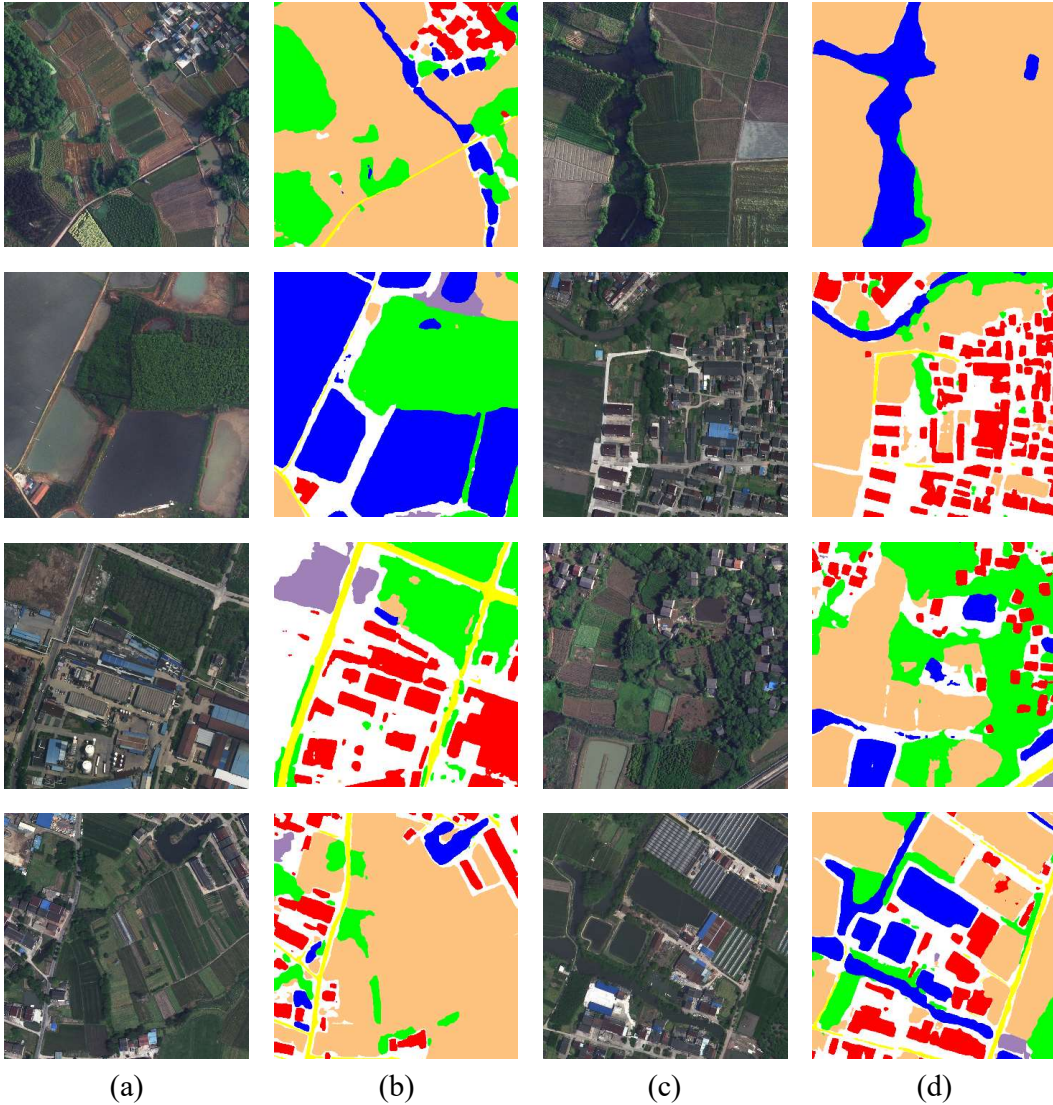4. *"Is there a label or target associated with each instance?"*

23

Figure 7: Visualization of SelectiveMAE predictions on the LoveDA testing set. (a)(c) Testing images. (b)(d) Predicted results of SelectiveMAE.

A: No, our dataset is intended for self-supervised learning. Therefore, each instance is an individual remote sensing image and does not contain annotations.

5. *"Is any information missing from individual instances?"*

    A: No.

6. *"Are relationships between individual instances made explicit (e.g., users' movie ratings, social network links)?"*

    A: Yes, the relationship between individual instances is explicit.

7. *"Are there recommended data splits (e.g., training, development/validation, testing)?"*

    A: Yes, the entire dataset is intended for self-supervised methods, and we recommend using the whole dataset for self-supervised learning research.

8. *"Is the dataset self-contained, or does it link to or otherwise rely on external resources (e.g., websites, tweets, other datasets)?"*

    A: Yes, our dataset relies on many publicly available remote sensing datasets, which we have detailed in the main text.

Figure 8: Visualization of SelectiveMAE predictions on the SpaceNetv1 testing set. (a)(c) Ground truth. (b)(d) Predicted results of SelectiveMAE.

9. *"Does the dataset contain data that might be considered confidential (e.g., data that is protected by legal privilege or by doctor–patient confidentiality, data that includes the content of individuals' non-public communications)?"*
   A: No, all data are clearly licensed.

10. *"Does the dataset contain data that, if viewed directly, might be offensive, insulting, threatening, or might otherwise cause anxiety?"*
    A: No.

7.5.3 Collection Process

In addition to the goals outlined in the previous section, the questions in this section are designed to elicit information that may help researchers and practitioners create alternative datasets with similar characteristics. Again, questions that apply only to datasets that relate to people are grouped together at the end of the section.

1. *"How was the data associated with each instance acquired?"*
   A: Please refer to the details listed in the main text Sec. 3.

2. *"What mechanisms or procedures were used to collect the data (e.g., hardware apparatuses or sensors, manual human curation, software programs, software APIs)?"*

25

A: Please refer to the details listed in the main text Sec. 3.

3. *"If the dataset is a sample from a larger set, what was the sampling strategy (e.g., deterministic, probabilistic with specific sampling probabilities)?"*

   A: Please refer to the details listed in the main text Sec. 3.

7.5.4 Preprocessing, Cleaning, and Labeling

The questions in this section are intended to provide dataset consumers with the information they need to determine whether the "raw" data has been processed in ways that are compatible with their chosen tasks. For example, text that has been converted into a "bag-of-words" is not suitable for tasks involving word order.

1. *"Was any preprocessing/cleaning/labeling of the data done (e.g., discretization or bucketing, tokenization, part-of-speech tagging, SIFT feature extraction, removal of instances, processing of missing values)?"*

   A: Yes, we preprocessed and cleaned data in our dataset.

2. *"Was the 'raw' data saved in addition to the preprocessed/cleaned/labeled data (e.g., to support unanticipated future uses)?"*

   A: Yes, raw data is accessible.

3. *"Is the software that was used to preprocess/clean/label the data available?"*

   A: Yes, the necessary software used to preprocess and clean the data is publicly available.

7.5.5 Uses

The questions in this section are intended to encourage dataset creators to reflect on tasks for which the dataset should and should not be used. By explicitly highlighting these tasks, dataset creators can help dataset consumers make informed decisions, thereby avoiding potential risks or harms.

1. *"Has the dataset been used for any tasks already?"*

   A: No.

2. *"Is there a repository that links to any or all papers or systems that use the dataset?"*

   A: Yes, we provide such links in our GitHub repository.

3. *"What (other) tasks could the dataset be used for?"*

   A: The dataset could be used for training the remote sensing foundation models with the self-supervised learning method.

4. *"Is there anything about the composition of the dataset or the way it was collected and preprocessed/cleaned/labeled that might impact future uses?"*

   A: N/A.

5. *"Are there tasks for which the dataset should not be used?"*

   A: N/A.

7.5.6 Distribution

Dataset creators should provide answers to these questions prior to distributing the dataset either internally within the entity on behalf of which the dataset was created or externally to third parties.

1. *"Will the dataset be distributed to third parties outside of the entity (e.g., company, institution, organization) on behalf of which the dataset was created?"*

   A: No.

2. *"How will the dataset be distributed (e.g., tarball on website, API, GitHub)?"*

   A: Very likely to be distributed by website, API, and GitHub repository.

3. *"When will the dataset be distributed?"*

   A: The datasets are publicly accessible.

4. *"Will the dataset be distributed under a copyright or other intellectual property (IP) license, and/or under applicable terms of use (ToU)?"*

   A: Yes, the dataset is under the Creative Commons Attribution-NonCommercial-ShareAlike 4.0 International License.

5. *"Have any third parties imposed IP-based or other restrictions on the data associated with the instances?"*

   A: No.

6. *"Do any export controls or other regulatory restrictions apply to the dataset or to individual instances?"*

   A: No.

7.5.7 Maintenance

As with the questions in the previous section, dataset creators should provide answers to these questions prior to distributing the dataset. The questions in this section are intended to encourage dataset creators to plan for dataset maintenance and communicate this plan to dataset consumers.

1. *"Who will be supporting/hosting/maintaining the dataset?"*

   A: The authors of this work serve to support, host, and maintain the datasets.

2. *"How can the owner/curator/manager of the dataset be contacted (e.g., email address)?"*

   A: The curators can be contacted via the email addresses listed on our webpage[5].

3. *"Is there an erratum?"*

   A: There is no explicit erratum; updates and known errors will be specified in future versions.

4. *"Will the dataset be updated (e.g., to correct labeling errors, add new instances, delete instances)?"*

   A: Yes, for the current version. Future updates (if any) will be posted on the dataset website.

5. *"Will older versions of the dataset continue to be supported/hosted/maintained?"*

   A: Yes. This is the first version of the release; future updates will be posted and older versions will be replaced.

6. *"If others want to extend/augment/build on/contribute to the dataset, is there a mechanism for them to do so?"*

   A: Yes, we provide detailed instructions for future extensions.

7.6 Limitation and Potential Societal Impact

In this section, we elaborate on the limitations and potential societal impact of this work.

7.6.1 Potential Limitations

While RS-4M provides a comprehensive benchmark for training the remote sensing foundation models with self-supervised learning methods, there are several limitations to consider:

- **Scope of Sensors:** Although our benchmark includes 4 million visible light remote sensing images, it may not cover all possible real-world scenarios. There could be additional sensor data, like multispectral data that were not included in this study, potentially limiting the generalizability of our findings.

- **Model and Dataset Diversity:** While our dataset is primarily focused on adapting to downstream tasks like detection and segmentation, there is undeniably less data available for these tasks compared to general scene classification. In the future, we should collect more data that is better suited for various downstream tasks.

- **Computation and Resource Requirements:** Pre-training on the extensive RS-4M dataset, comprising 4 million images, demands substantial computational resources, despite our introduction of the efficient SelectiveMAE method. This may limit access to the benchmark for research groups lacking ample computational power.

---

[5] https://github.com/Fengxiang23/SelectiveMAE.

7.6.2 Potential Negative Societal Impact

While the development of remote sensing foundation models with self-supervised learning methods has the potential to significantly advance remote sensing downstream tasks, there are potential negative societal impacts that must be considered:

- **Safety Risks:** Our benchmark aims to improve remote sensing foundation models, but relying too heavily on these models may breed overconfidence in autonomous systems. It's crucial to deploy these systems with adequate safety measures and human oversight to uphold public safety.

- **Environmental Impact:** Training and evaluating remote sensing foundation models demand substantial computational resources, leading to a notable environmental footprint. Encouraging the adoption of energy-efficient algorithms (*i.e.*, the proposed SelectiveMAE) and sustainable computing practices is crucial to reduce the environmental impact of this research.

- **Bias and Fairness:** The performance of foundational remote sensing models can vary across different environments and conditions, potentially introducing biases in downstream tasks within the remote sensing domain. It is essential to train and evaluate these models on diverse datasets to ensure fairness and avoid discriminatory outcomes.